MOLECULAR IMAGING AND BIOLOGY

Mol Imaging Biol (2019) 21:945–953
DOI: 10.1007/s11307-019-01319-4

Published Online: 21 February 2019

WMIS World Molecular Imaging Society

Check for updates

RESEARCH ARTICLE

(2S,4R)-4-[^{18}F]Fluoroglutamine as a PET Indicator for Bone Marrow Metabolism Dysfunctional: from Animal Experiments to Clinical Application

Hua Zhu,[1] Fei Liu,[1] Yan Zhang,[2] Jianhua Yang,[1] Xiaoxia Xu,[1] Xiaoyi Guo,[1] Teli Liu,[1] Nan Li,[1] Lin Zhu,[2,3] Hank F. Kung,[3,4] Zhi Yang[1]

[1]*Key Laboratory of Carcinogenesis and Translational Research (Ministry of Education/Beijing), Department of Nuclear Medicine, Peking University Cancer Hospital & Institute, Beijing, 100142, China*

[2]*Key Laboratory of Radiopharmaceuticals, Ministry of Education, Beijing Normal University, Beijing, 100875, China*

[3]*Capital Medical University, Beijing Institute for Brain Diseases, Beijing, 100069, China*

[4]*Department of Radiology, University of Pennsylvania School of Medicine, 3700 Market Street, Suite 305, Philadelphia, PA, 19104, USA*

Abstract

Purpose: Previous reports confirmed that (2S,4R)-4-[^{18}F]Fluoroglutamine ([^{18}F]GLN) accumulated in bone and bone marrow. This study investigates the potential of using [^{18}F]GLN positron emission tomography (PET) to monitor changes of bone marrow activity after chemotherapy (myelosuppression).

Procedures: Bone marrow inhibition model in mice was induced by an intravenous injection of chemotherapy drug (doxorubicin or rituximab) and the inhibition was confirmed by routine blood cell counts. Bone uptakes of these four radiotracers (2-deoxy-2-[^{18}F]fluoro-D-glucose, [^{18}F]GLN, 3′-dexoy-3′-[^{18}F]fluorothymidine ([^{18}F]FLT), and sodium [^{18}F]fluoride) in the mice were measured after i.v. injection and dissection of femur and tibia, and the uptakes in bone-only (BO) and bone marrow (BM) were obtained after separating bone from bone marrow. Additionally, six volunteers were recruited and evaluated with [^{18}F]GLN. The PET-/CT-guided volumes of interests (VOI) in cervical, thoracic, lumbar vertebra, and skull cortical bone were defined as bone marrow or bone for evaluation, respectively.

Results: [^{18}F]GLN showed a relatively high bone marrow uptake in mice (up to 9.5 ± 1.3 % ID/g) at 1 h after injection, which was 2.1 times that of [^{18}F]FLT. The [^{18}F]GLN uptakes in the bone marrow were substantially inhibited by chemotherapy drug. The decrease of [^{18}F]GLN's bone marrow uptake was consistent with the reduction of white blood cells (myelosuppression). For [^{18}F]GLN/PET imaging in humans, the SUV_{mean} value of bone marrow (1 h after i.v. injection) was between 3.1 and 3.6 in the healthy volunteers ($n = 3$), and between 1.8 and 2.2 ($n = 3$) ($P < 0.001$) in myelosuppression patients, showing a clear reduction of bone marrow uptake.

Conclusions: Dissection experiments in mice showed that [^{18}F]GLN displayed relatively high bone marrow uptake, and the uptake was sensitive to bone marrow inhibition induced by

Electronic supplementary material The online version of this article (https://doi.org/10.1007/s11307-019-01319-4) contains supplementary material, which is available to authorized users.

Correspondence to: Hank Kung; *e-mail:* kunghf@gmail.com, Zhi Yang; *e-mail:* pekyz@163.com

doxorubicin/rituximab. The same conclusion was confirmed [18F]GLN/PET imaging in humans. Therefore, [18F]GLN/PET imaging may be a useful tool to assess reduction of bone marrow activity in cancer patients, who may be at risk of myelosuppression after chemotherapy.
Trial Registration: Approved by Institutional Review Board of Peking University Cancer Hospital (No. 2017KT38). Registered 18 August 2017.

Key words: (2S,4R)-4-[18F]fluoroglutamine, Bone marrow, Glutamine metabolic imaging, Myelosuppression

Introduction

Myelosuppression, also known as bone marrow suppression, is a common side effect of chemotherapy that is characterized by declining production of blood cells (including red blood cells, white blood cells, and platelets). Early and noninvasive detection of reducing bone marrow activity in cancer patients under chemotherapy is clinically important and useful for managing treatment. Currently, peripheral smear examination, bone marrow biopsy, and magnetic resonance imaging are often required to make an accurate diagnosis [1]. However, these methods are always individually dependent, and some are highly invasive, therefore, may not be suitable for every patient. Functional bone marrow abnormality may precede conventional laboratory examination and radiographic findings. An alternative technique for assessing myelosuppression would be highly valuable.

Traditionally, radio-labeled iron and [99mTc]sulfur colloid have been used as effective agents to estimate both volume, location, and function of bone marrow by imaging with a gamma camera [2–4]. Molecular imaging, especially positron emission tomography (PET), offers a convenient and sensitive method to view the whole body distribution of bone marrow and monitor its changes after chemotherapy. Previously, 3′-Deoxy-3′-[18F]-fluorothymidine ([18F]FLT), a thymidine analog, can directly incorporate into new deoxyribonucleic acid (DNA) synthesis during cell proliferation, including blood cells [5]. It is well documented that [18F]FLT can directly visualize functional marrow distribution in patients including tumor proliferation and chemotherapy response in bone marrow [6–8]. Additionally, 2′-Deoxy-2′-[18F]-fluoro-D-glucose ([18F]FDG) is the most widely used PET tracer to image the upregulation of glucose metabolism in tumors. Theoretically, [18F]FDG holds great potential as a bone marrow-monitoring agent, due to not only its extensive clinical utilization but also its strong association with cellular glucose metabolism. Changes in [18F]FDG uptake in bone marrow of patients with Hodgkin disease after cytotoxic chemotherapy have been reported in several clinical studies [9, 10]. However, the results of these studies were not consistent, and the relatively low bone tissue uptake of [18F]FDG also limits its further application as bone marrow detection agents.

It has been reported that L-glutamine is an alternative source of metabolic substrate for proliferating cells and it also provides building blocks for DNA/protein synthesis [11]. We reasoned that the functional bone marrow PET scan based on [18F]glutamine might detect changes prior to abnormalities measured by currently employed Tc-99m bone scans and other radiographic imaging methods. We have recently developed and prepared an optically pure (2S,4R)-4-[18F]fluoroglutamine ([18F]GLN), an analog of glutamine, that exhibits specific uptake in animal models [12, 13]. Previous studies have demonstrated that [18F]GLN holds great promise to study solid tumor (glioma, breast cancer, etc.) by PET imaging [14–16]. High accumulation of [18F]GLN in bone and bone marrow has attracted our attention, because changes in glutamine metabolism might serve as a platform to develop new imaging agents for evaluating bone marrow activity. Glutamine-based PET imaging agent [18F]GLN might be useful as a bone marrow detection agent in assessing the side effects of chemotherapy.

We report herein the results of evaluating [18F]GLN as a novel radiotracer to study myelosuppression after chemotherapy. We first investigated bone marrow uptake of [18F]GLN in mouse by dissection and counting methods. We further translate this [18F]GLN/PET imaging agent to measure bone marrow activity in healthy volunteers and cancer patients with myelosuppression.

Materials and Methods

All animal procedures used in this research followed the guidelines of the Institutional Animal Care and Use Committee of Peking University Cancer Hospital (Beijing, China). Blood smears were scanned on an Advia 2120 hematology analyzer (Siemens, Germany) ScanScope XT slide scanner (× 20) (Aperio, CA, USA). Counting of neutrophils, lymphocytes, eosinophils, basophils, monocytes, and platelet was performed on eight × 10 fields with the ImageScope software (Leica Biosystems, Germany).

Production of [18F]GLN, [18F]FLT, [18F]NaF, and [18F]FDG Radiotracers

Sodium [18F]fluoride (Na[18F]F) was produced by Sumitomo HM-20 cyclotron (20 MeV, Sumitomo Heavy Industries, Ltd., Tokyo, Japan). The production of [18F]GLN was performed at Peking University Cancer Hospital

cyclotron center as previously reported with some modifications [13]. The radiochemical and stereochemical purity of the final product was determined by chiral high-performance liquid chromatography (HPLC). The retention time for the (2S,4R)-isomer was at 14.5 min, while that of the inactive (2R,4R) isomer was at 21.4 min, with less than 5 % (Suppl, Fig. S1, see Electronic Supplementary Material (ESM)). [18F]FLT synthesis kits were purchased from ABX (Radeberg, Germany). [18F]FDG and [18F]FLT were synthesized on a multi-functional radio-synthesizer module. [18F]FDG and Na[18F] F were obtained from daily productions at Peking University Cancer Hospital.

Micro-PET Imaging

Micro-PET imaging studies were conducted with [18F]GLN, [18F]FDG (6 h fasting before [18F]FDG PET imaging), [18F]FLT, and Na[18F]F on dedicated Micro-PET/CT equipment (Super-Argus, SEDECAL, Spain) that has a field of view of 12.0 cm. Both Kunming mice ($n = 5$ for each group) and rat ($n = 3$ for each group) were used for the imaging studies (Beijing Vital River Laboratory Animal Technology Co., Ltd., Beijing, China). All animals were subjected to isoflurane anesthesia (1–2 %, 1 l/min oxygen) and were then placed on a temperature self-adjust tube to maintain body temperature throughout the procedure. Animals were visually monitored for breathing and any other signs of distress throughout the entire imaging period. Kunming mice were injected with 18.5 MBq of each radiotracer and rats were injected with 55.5 MBq [18F]GLN, respectively. Data acquisition began after an intravenous injection of the Radiotracer. All scans were conducted over a period of 2 h (dynamic, 5 min/frame) (Suppl. Fig. S2, see ESM). CT fusion was also conducted in the Micro-PET analysis system. The images were reconstructed using a three-dimensional ordered subsets expectation maximum algorithm (OSEM) without attenuation correction.

In vivo Bone Tissue Distribution Studies in Mice

To each mouse, 1.85 MBq of either [18F]GLN, [18F]FDG, [18F]FLT, or Na[18F] F was injected intravenously ($n = 6$ for each group) when it was under isoflurane anesthesia (2.5 %, 1 mL/min oxygen). The bone marrow inhibition mouse model ($n = 6$) was created by intravenously injection of doxorubicin (DO) (50 mg/kg, LC laboratories, Woburn, USA) or Rituximab (Rit) (50 mg/kg, Roche, USA) at 24 h before [18F]GLN injection. The myelosuppression in these treated mice was confirmed by routine blood test, including routine complete blood count (CBC), routine white blood cell (WBC) differential, additional routine parameters, and platelet test ($n = 5$), as shown in Suppl Fig. S3 and Table S1 (see ESM).

Control and treated mice were sacrificed at 1 h after radiotracers injection, the lower leg bone, used to represent total bone (TB), was removed, weighted, and counted with a γ-counter (Perkin Elmer, Waltham, MA, USA) immediately. Bone marrow (BM) was carefully swiped and collected by an absorbent paper from the crushed bone, making sure that none of the wet bone morrow remained in the bone. The bone marrow-free bone was designated as bone-only (BO) (Suppl Fig. S4, see ESM). BO were also weighted and counted with a γ-counter. The weight of BM can be calculated from the following equation: BM = TB – BO, and the radioactivity counts of BM were measured by a γ-counter. The % ID/g values of TB, BO, and BM were calculated using 1 % radiotracer as standard for each tracer and each group.

Subject Enrollment

This clinical study was approved by the Institutional Review Board of Peking University Cancer Hospital (No. 2017KT38). All subjects ($n = 6$) signed a written informed consent form prior to the study. Exclusion criteria included mental illness, severe liver or kidney disease with serum creatinine greater than 3.0 mg/dl (270 mM), and hepatic enzyme level five times that of normal value. Participants were also excluded if they were known to have severe allergy, hypersensitivity to intravenous radiographic contrast agents, and claustrophobia during PET/CT scanning, and if they were pregnant or breast-feeding. Typical health information of participants and their WBC analysis data are shown in Table 1. Three healthy volunteers (HV) and three myelosuppression patients (MP) were recruited for this study.

[18F]GLN PET/CT Scanning Procedures and VOI-Based SUV Analysis

The blood pressure, pulse, respiratory frequency, and body temperature were regularly measured. Any possible side effects during [18F]GLN PET/CT scanning and within 1 week after the examination were collected and analyzed for safety.

No specific preparation for participants was requested on the day of [18F]GLN PET/CT scanning. Six successive whole body PET/CT scans were obtained on a Biograph mCT Flow 64 scanner (Siemens, Erlangen, Germany). Whole body scans (from the top of skull to the middle of femur) of each volunteer were acquired by a continuous movement of the patient bed. A dose of [18F]-GLN at 185–259 MBq (3.7 MBq/Kg) was injected intravenously, followed by serial whole body dynamic PET acquisitions (0–60-min dynamic scan).

A Siemens MMWP workstation was used for clinical PET/CT imaging reconstruction. [18F]GLN PET/CT images were transferred to the Eclipse™ treatment planning system at version 13.6 (Varian medical system, Palo Alto, CA, USA). Quantification of [18F]GLN uptake in bone and bone

Table 1.. Participants' health information and typical white blood cells (WBC) test result analysis

No.	1	2	3	4	5	6
Participants	Healthy volunteers ($n = 3$)			Myelosuppression patient ($n = 3$)		
Cancer type	None	None	None	Esophageal cancer	Cervical cancer	Cervical cancer
Myelosuppression	Normal	Normal	Normal	Stage 3	Stage 2	Stage 3
Year	50	47	50	77	45	55
Sex	Male	Female	Female	Male	Female	Female
WBC	7.9×10^9/l	6.9×10^9/l	5.9×10^9/l	No data	2.1×10^9/l (↓)	2.0×10^9/l (↓)
Neutrophil	6.0×10^9/l	4.7×10^9/l	4.3×10^9/l	No data	1.5×10^9/l	0.4×10^9/l
Lymphocyte	1.5×10^9/l	1.7×10^9/l	1.2×10^9/l	No data	3.1×10^8/l	1.4×10^9/l
Monocyte	4.1×10^8/l	3.3×10^8/l	3.2×10^8/l	No data	2.2×10^8/l	2.3×10^8/l
Eosinophil	7.2×10^7/l	1.4×10^8/l	1.2×10^8/l	No data	4.0×10^7/l	2.0×10^7/l
Basophil	7.9×10^7/l	1.3×10^7/l	3.0×10^7/l	No data	$< 1 \times 10^5$ /l	1.2×10^7/l

marrow was performed using a volume of interested (VOI) quantification analysis method, and the mean standard uptake [$SUV(s)_{mean}$] values were calculated and averaged. The largest VOI in the 3rd to 7th cervical vertebra, 1st to 12th thoracic vertebra, and 1st to 5th lumbar vertebra (defined as bone marrow) were drawn on the PET/CT images and their positions were verified by corresponding CT images. The volumes of interest on PET images for bone marrow/bone from different segments (cervical, thoracic, and lumbar region) of spine are shown in Fig. 4 and Suppl. Fig. S5–6 (see ESM). Bone-only segment was obtained by drawing a region of bone in the skull.

Statistical Analysis

Percentage of injected dose per gram of tissue was calculated and presented as the mean ± standard deviation. Bone tissue distribution data were analyzed using two-tailed, unpaired student *t* tests, with *P* values less than 0.05 considered to be statistically significant. These statistical computations were performed using the Excel software program (Microsoft Corporation, Redmond, WA) or Graphpad software (Graphpad prism 5).

Ddata Availability

All data generated or analyzed during this study are included in this published article [and its supplementary information files]. Additional datasets used and/or analyzed during the current study are available from the corresponding author on reasonable request.

The datasets supporting the conclusions of this article are available in the Beijing Cancer Hospital Nuclear Medicine Department Medical Records Room data base (Beijing, China) repository.

Results

Micro-PET Study of Each Radiotracers in Mice

Micro-PET images (coronal and sagittal position) of Kunming mice obtained at 1 h after each radiotracers injection are shown in Fig. 1. Na[^{18}F] F provides a general view of skeleton uptake with high spatial resolution. While [^{18}F]GLN exhibits mainly whole body bone tissue metabolism and low main organ (brain, neck, chest, and abdomen) uptake, indicating either defluorination or BM uptake. [^{18}F]FLT's uptake is observed in the spleen, liver, kidney, and bladder, and in the bone tissues (mainly BM). [^{18}F]FDG is a well-known radiotracer for the glucose metabolism pathway imaging, the main uptake shown in the heart, brain, and some muscle tissues, it demonstrates lower uptake in skeleton.

Here, Na[^{18}F] F showed standard skeletal uptake and [^{18}F]FLT exhibits typically BM uptake. Micro-PET imaging of [^{18}F]GLN in mice showed the intermediate state between Na[^{18}F] F and [^{18}F]FLT. White arrows (numbered 1–5) indicate differences between Na[^{18}F] F, [^{18}F]GLN, and [^{18}F]FLT in bone tissues, also shown in Fig. 1.

Dynamic Micro-PET studies were conducted with [^{18}F]GLN on rat shown in Figure S2. The representative static slice of 5–30 min sagittal images (Figure S2) and time-activity curves for assessing spine metabolism kinetics were generated by drawing regions of interest. The kidney uptake gradually decreased with the extension of time at 5 min after injection means the metabolism of [^{18}F]GLN. The heart uptake almost keeps the same level from 5 to 30 min indicating that [^{18}F]GLN may have a stable blood circulation time. The spine can be gradually visualized after 10 min of injection, and the lower spine (LS) has accumulated more radiotracer compared with the upper spine (US). Slight increasing uptake in LS and US can be observed. The brain uptake keeps at low level compare with an increasing uptake in the skull.

Bone Tissue Biodistribution Studies of Radiotracers in Mice

The *ex vivo* biodistribution studies of [^{18}F]GLN, [^{18}F]FDG, [^{18}F]FLT, and Na[^{18}F] F were performed in normal mice. The distribution of radioactivity in bone tissues (tibia and femur) after injection of each tracer at 60 min are summarized in Fig. 2a. The TB uptakes of [^{18}F]GLN, [^{18}F]FDG, [^{18}F]FLT, and Na[^{18}F] F were 15.7 ± 1.3 % ID/g, 2.1 ± 0.3 % ID/g, 3.7 ± 0.1 % ID/g, and 48.1 ± 2.4 % ID/g,

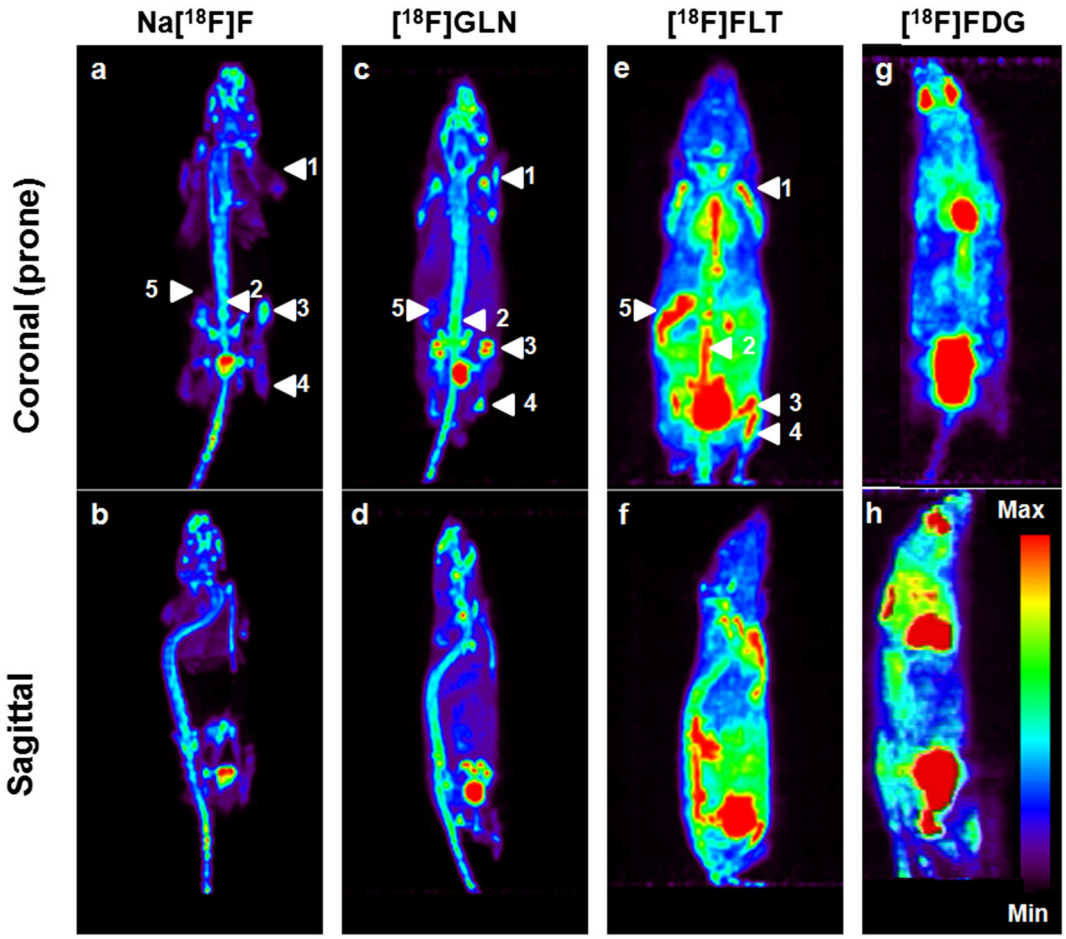

Fig. 1. Maximum intensity projection images of a, b Na[^{18}F]F; c, d [^{18}F]GLN; e, f [^{18}F]FLT; and g, h [^{18}F]FDG, respectively, in normal Kunming mice by micro-PET equipment at 1 h after intravenous injection (injection dose 18.5 MBq for each radiotracer). White arrows on coronal MIPs are 1, forelimb; 2, lower spine; 3, upper hindlimb; 4, lower hindlimb; 5, spleen.

respectively. The Na[^{18}F] F showed the highest TB uptake, while that of [^{18}F]FDG was the lowest. The uptake of [^{18}F]GLN was about five times that of [^{18}F]FLT. The BM uptakes of [^{18}F]GLN, [^{18}F]FDG, [^{18}F]FLT, and Na[^{18}F]F were 9.5 ± 1.3 % ID/g, 1.8 ± 0.8 % ID/g, 4.5 ± 0.4 % ID/g, and 7.7 ± 1.2 % ID/g, respectively. [^{18}F]GLN showed the highest BM uptake, which was more than two times that of [^{18}F]FLT. [^{18}F]FDG also showed the lowest BM uptake. Two chemotherapy drugs, DO and Rit were selected to induce myelosuppression by injecting intravenously to Kunming mice using the dose of 50 mg/kg at 24 h prior to the [^{18}F]GLN biodistribution studies. The bone marrow inhibitions in mice were confirmed by routine blood test using blood collected from those mice ($n = 4$). Three groups of mice were sacrificed at 1 h after radiotracers injection, and the % ID/g values of femur and tibia ($n = 6$), including TB, BO, and BM were measured and calculated. As shown in Fig. 2b, all three groups showed similar TB uptakes (from 13.9 ± 2.0 to 16.0 ± 3.0 % ID/g) and BO uptakes (from 17.4 ± 3.5 to 18.8 ± 4.1 % ID/g). Both DO and Rit inhibited the bone marrow uptakes of [^{18}F]GLN, with those of 3.9 ± 1.1 % ID/g and 5.7 ± 0.8 % ID/g, respectively, in the treated mice. In this study, [^{18}F]GLN showed the highest bone marrow uptake among the four radiotracers, and the largest uptake reduction after treatment with chemotherapy drugs in the mouse model. Therefore, [^{18}F]GLN holds promise as a novel noninvasive myelosuppression detecting PET radioligand.

Time-Dependent Bone and Bone Marrow Uptake of [^{18}F]GLN/PET in Humans

In human clinical PET/CT imaging, the uptake of bone tissue steadily increased over time from 0 to 60 min post injection, as shown in Fig. 3. [^{18}F]GLN displayed higher bone marrow uptake than bone tissue in PET-/CT-guided and VOI-based quantitative analysis, as shown in Fig. 3. The mean standard uptake values [SUV(s)$_{mean}$] of bone-only at 10, 20, 30, 40, 50, and 60 min, were 0.52 ± 0.15, 0.63 ± 0.11, 0.61 ± 0.16, 0.72 ± 0.25, 0.80 ± 0.26, 0.81 ± 0.39, and 0.92 ± 0.43 % ID/g, respectively. The mean standard uptake values [SUV(s)$_{mean}$] of bone marrow at 10, 20, 30, 40, 50, and 60 min were 2.44 ± 0.16, 2.74 ± 0.29, 2.78 ± 0.09, 2.90 ± 0.18, 2.95 ± 0.06, and 3.03 ± 0.01 % ID/g, respectively. On average, bone marrow

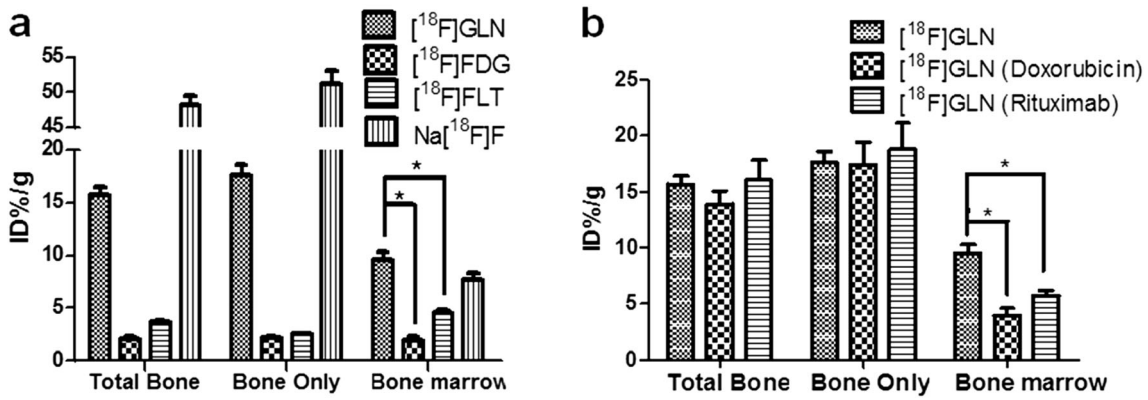

Fig. 2. Biodistribution of [18F]GLN, [18F]FDG, [18F]FLT, and Na[18F] F in normal and treated (DO or Rit) mice. **a** Radiotracer's uptake in bone tissue. Radioactivity in total bone (TB), bone-only (BO), and bone marrow (BM), respectively, **b** [18F]GLN's uptake in each bone tissues, including in control-, DO-, and Rit-treated groups, respectively. Single asterisk indicates $P < 0.001$.

uptake was 3.03 ± 0.01 % ID/g, which was 3.3 times of bone-only uptake at 60 min in control subjects.

Using clinical PET VOI-based quantification analysis (Fig. 4), [18F]Gln gradually accumulated in the bone marrow of cervical, thoracic, and lumbar vertebra in three healthy controls, with [$SUV(s)_{mean}$] from 3.1 to 3.6 (Fig. 5). Myelosuppression patients ($n = 3$) showed reduced [18F]Gln uptakes in the bone marrow of the corresponding regions. The average $SUV(s)_{mean}$ was 2.0 ± 0.2. Significant difference ($P < 0.001$) in bone marrow uptakes was observed in healthy volunteers (HV) and myelosuppression patient (MP). The skull cortical bone (bone-only) in both healthy volunteers and myelosuppression patients exhibited similar uptakes, with the average SUV_{mean} from 0.4 to 1.0.

Discussion

Myelosuppression is a disease associated with deficiencies in the ability of bone marrow to produce blood cells: platelets, red blood cells, and white blood cells. It is often caused by side effects of cancer chemotherapy and radiation therapy. During the period of myelosuppression, patients may be at an increased risk of infection (due to neutropenia) or bleeding or may experience symptoms of anemia (reduction of red blood cells) [17–21]. Specific causes of myelosuppression may be related to several events during chemotherapy. Firstly, it is commonly related to drug-induced rapid killing of dividing cells including stem cells in the bone marrow. This situation is more often encountered and exacerbated during treatment (*via* chemotherapy or radiation), especially in various cancer patients whose disease are not hematology-related. These patients show progressively increased side effect of treatments leading to myelosuppression. Secondly, it may also be caused by cancers of bone marrow, such as leukemia, lymphoma, and myeloma metastatic cancer, which resulted in "crowing out" effects of blood cell production. Thirdly, it is also likely due to deliberate myeloablation of hematology-related cancer patients by high-dose chemotherapy. The latter two events are directly related to hematological cancers, while they are clinically important. However, the detection of myelosuppression in these conditions is not the major concern for this work. Monitoring myelosuppression by PET imaging is clinically important for management of cancer patient and providing critical

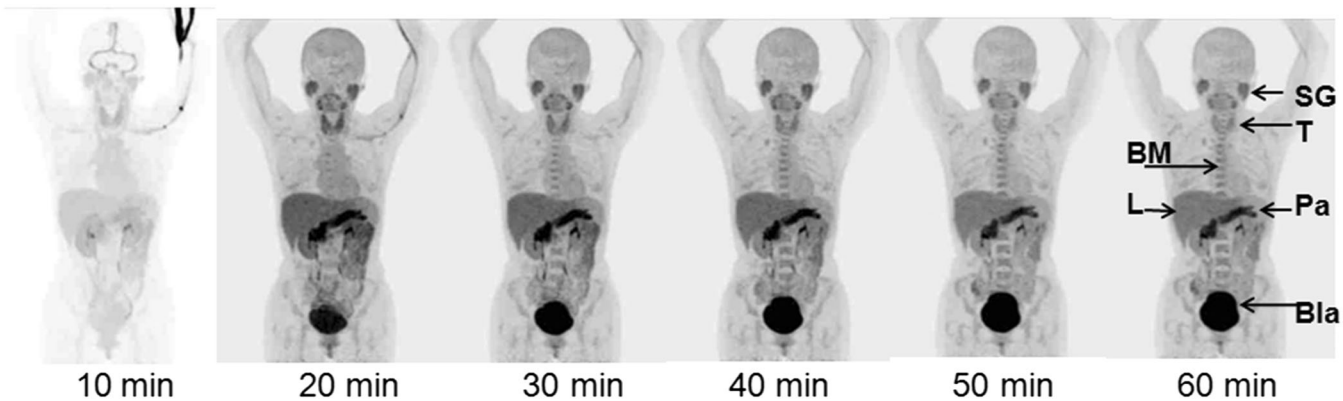

Fig. 3. Whole body maximum-intensity-projection PET images of a normal volunteer at 10, 20, 30, 40, 50, and 60 min were obtained by dynamic scans after intravenous administration of 185 MBq [18F]GLN in a 47-year-old female. SG salivary gland, T thyroid, L liver, Pa pancreases, Bla bladder, BM bone marrow.

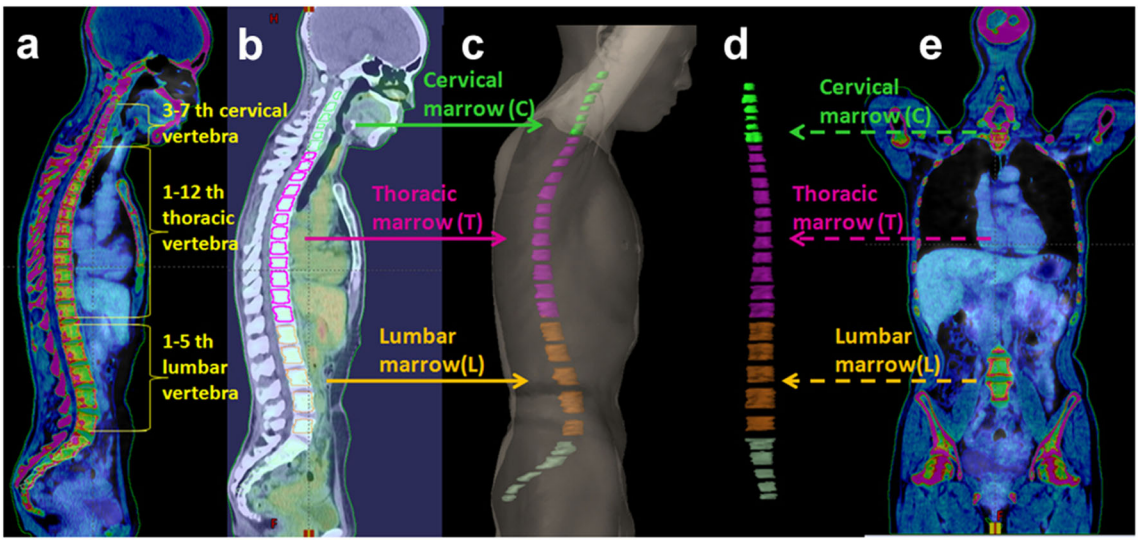

Fig. 4. PET-/CT-based volume of interest (VOI) for each region was defined. a Illustration of PET/CT sagittal plane of defined cervical, thoracic, and lumbar vertebra, b PET-/CT-guided VOI-based quantification of cervical, thoracic, and lumbar bone marrow area. c Sagittal plane reconstructed bone marrow in human subjects. d Coronal plane of reconstructed bone marrow in same subject. e Illustration of PET/CT coronal plane of defined cervical, thoracic, and lumbar vertebra. Solid lines in each color indicate the actual position of each bone marrow and dotted lines indicate the position of each vertebra.

information for titrating cancer therapy doses. Previously, [18F]FDG and [18F]FLT have been evaluated as myelosuppression imaging agents. Low and variable bone tissue uptake of [18F]FDG limits its further application as bone marrow radiotracer [10, 12]. [18F]FLT, a thymidine analog, appears to be a non-invasive tool to monitor the distribution of proliferating bone marrow in patients. As [18F]FLT cellular uptake only reflects thymidine kinase (TK1) activity, challenges remain to fully predicate the reduction of bone marrow metabolic activity after chemotherapy.

Glucose is the most common source of nutrient in normal cells, and glucose generates energy *via* aerobic metabolism (TCA cycle in the mitochondria). In certain cancer cells due to various mutations and the unmet needs for high metabolic energy, glucose is use as fuel in a less efficient anaerobic glycolysis. This phenomenon is commonly referred to as the "Warburg" effect. Additional adaptation of cancer cells (and sometimes also occurring in fast-dividing cells) will switch to use glutamine as a source for energy production. Glutamine plays an important role in proliferation, especially in cancer cells. Changes in cellular metabolic mechanism are essential in order to adapt to glutamine metabolism, which is an important functional adjustment of fast-growing cells. Previously, [18F]GLN/PET has been evaluated in animal and humans as a potential imaging agent for studying glutamine metabolism in cancer cells [13–15, 22, 23].

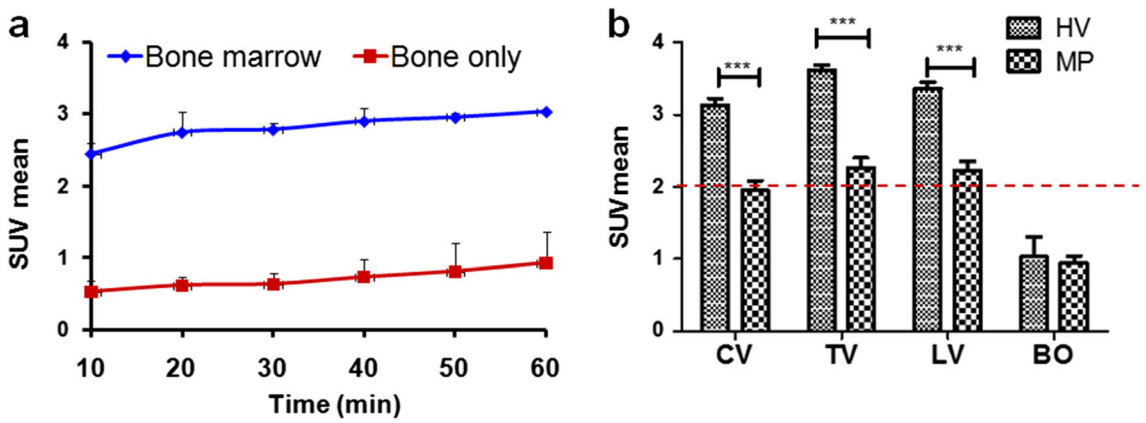

Fig. 5. **a** SUVmean analysis of bone and bone marrow tissue in PET/CT imaging of three healthy volunteers ($n = 3$). **b** Comparison of bone marrow uptake in healthy volunteers (HV) and myelosuppression patient (MP) ($n = 3$) at 60 min after [18F]GLN injection. CV, TV, LV, and BO indicate cervical vertebra, thoracic vertebra, lumbar vertebra, and bone-only respectively. Triple asterisks indicate $P < 0.0001$. Red dash line indicates the SUV_{mean} value 2.0 as a cut-off line, which separated HV from MP patients.

In this study, we have demonstrated that in normal mice, [18F]GLN showed relatively high bone marrow uptake, which was up to 2.1 times of [18F]FLT. Chemotherapy drugs, such as DO [24–26] and Rit [27–29], substantially inhibited the bone marrow uptake of [18F]GLN. Mice's bone tissues are too tiny to be actually quantified by Micro-PET, we used rat for time-dependent bone tissue metabolism study. The rat's spine can be gradually visualized after 10 min of injection, and the lower spine (LS) have accumulated more radiotracer comparing with upper spine (US). A slight increasing of the tracer in both LS and US can be observed. These observations provided an opportunity in developing [18F]GLN/PET as a tool for studying changes in bone marrow function after cancer therapy. It is possible that the stem cells in the bone marrow may be more sensitive to chemotherapy drugs leading to changes in the uptake of [18F]GLN. Normally, stem cells in the bone marrow are fast-dividing and rapidly growing cells. Certain aspects of stem cells' growth and proliferation are similar to cancer cells; they require increasing supply of metabolic energy and replenishing intermediates for metabolic pathway (anaplerosis). The unmet needs of such metabolic energy and building blocks may be supplemented by using glutamine, the most abundant amino acid available in the blood circulation. As such, these stem cells may have acquired gene mutations or built-in mechanisms to preferentially transport glutamine or [18F]GLN into the fast-growing cells. Side effects of chemotherapy may be reflected in a diminution of uptake of glutamine or [18F]GLN by these fast-dividing cells in the bone marrow.

It is also entirely possible that some of the uptake may be associated with the uptake in the bone (hydroxyapatite) due to [18F] fluoride after *in vivo* metabolism of the parent [18F]GLN probe [30]. However, at least in the mouse model, the reduction of bone marrow uptake was likely due to the reduced [18F]GLN uptake and retention, and it may not be due to binding of the fluoride ion to the hydroxyapatite. Results lend support for using this tracer as a probe for monitoring changes in bone marrow function. It would be necessary to further evaluate the potential of using [18F]GLN to evaluate the changes of bone marrow uptake in a larger group of cancer patients, who may have a lower stem cell activity in bone marrow after chemotherapy. One other unanswered question is that if the reduced [18F]GLN uptake in bone marrow is specifically related to glutamine metabolism; or perhaps, other 18F-labeled amino acids, such as [18F]fluoroethltyrosine or [18F]Fluciclovine, may also show the same propensity to changes in bone marrow function.

Conclusion

In summary, [18F]GLN showed high uptake in normal bone marrow and the uptake was significantly reduced after chemotherapy treatment in a mouse model and cancer patients. Imaging studies using [18F]GLN/PET may provide a direct and sensitive method to detect myelosuppression prior to symptomatic events, such as leukopenia or anemia, in patients undergoing chemotherapy.

Acknowledgments. We appreciates Peking University Cancer Hospital cyclotron team for providing each radiotracer.

Authors' Contributions. HZ, HFK, and ZY made the concept and designed the research. HZ, FL, and XXX developed the methodology. FL, YZ, TLL, and JH Y acquired data (labeling, animals, facilities, *etc.*). ZY XYG and XXX analyzed and interpreted data (*e.g.*, statistical analysis, ROI-quantification). HZ NL, LZ, HFK, and ZY wrote and reviewed the manuscript. HFK and ZY supervised this study. All authors read and approved the final manuscript.FundingThis work was supported in part by grants from the Beijing Natural Science Foundation Key Program (No. 7171002), this funding supports the clinical translational studies. And National Natural Science Foundation of China Projects (81671733, 81501519 and 81571705), those funding supports experiment researches.

Compliance with Ethical Standards

Ethics Approval and Consent to Participate

Inclusion of human participants and use of human data and human tissue in this study were approved by the Ethics Committee of Peking University Cancer Hospital. The use of animals in this study was approved by the animal research committee in Peking University Cancer Hospital. This clinical study was approved by the Institutional Review Board of Peking University Cancer Hospital (No. 2017KT38). Enrollment begins from 18 August 2017 to 30 December 2018. URL: not applicable.

Competing Interests

The authors declare that they have no conflict of interest.

Consent for Publication

Not applicable.

Publisher's Note. Springer Nature remains neutral with regard to jurisdictional claims in published maps and institutional affiliations.

References

1. Dietmar PB, Monika E, Hartmut H, Roland M (2008) Concise manual of hematology and oncology. Springer, New York, pp 802–822
2. Knospe WH, Rayudu VM, Cardello M et al (1976) Bone marrow scanning with 52iron (52Fe). Regeneration and extension of marrow after ablative doses of radiotherapy. Cancer 37:1432–1442
3. Desai AG, Thakur ML (1985) Radiopharmaceuticals for spleen and bone marrow studies. Semin Nucl Med 15:229–238
4. Siddiqui AR, Oseas RS, Wellman HN et al (1979) Evaluation of bone-marrow scanning with technetium-99m sulfur colloid in pediatric oncology. J Nucl Med 20:379–386
5. Bading JR, Shields AF (2008) Imaging of cell proliferation: status and prospects. J Nucl Med 49:64S–80S
6. Hayman JA, Callahan JW, Herschtal A, Everitt S, Binns DS, Hicks RJ, Mac Manus M (2011) Distribution of proliferating bone marrow in adult cancer patients determined using FLT PET imaging. Int J Radiat Oncol Biol Phys 79:847–852
7. Leimgruber A, Moller A, Everitt SJ, Chabrot M, Ball DL, Solomon B, MacManus M, Hicks RJ (2014) Effect of platinum-based chemoradiotherapy on cellular proliferation in bone marrow and spleen, estimated by 18F-FLT PET/CT in patients with locally advanced non-small cell lung cancer. J Nucl Med 55:1075–1080
8. Campbell BA, Callahan J, Bressel M, Simoens N, Everitt S, Hofman MS, Hicks RJ, Burbury K, MacManus M (2015) Distribution atlas of proliferating bone marrow in non-small cell lung cancer patients measured

by FLT-PET/CT imaging, with potential applicability in radiation therapy planning. Int J Radiat Oncol Biol Phys 92:1035–1043
9. Moulin-Romsee G, Hindié E, Cuenca X, Brice P, Decaudin D, Bénamor M, Brière J, Anitei M, Filmont JE, Sibon D, de Kerviler E, Moretti JL (2010) ^{18}F-FDG PET/CT bone/bone marrow findings in Hodgkin's lymphoma may circumvent the use of bone marrow trephine biopsy at diagnosis staging. Eur J Nucl Med Mol Imaging 37:1095–1105
10. Kostakoglu L, Goldsmith SJ (2003) ^{18}F-FDG PET evaluation of the response to therapy for lymphoma and for breast, lung, and colorectal carcinoma. J Nucl Med 44:224–239
11. Wasa M, Bode BP, Abcouwer SF, Collins CL, Tanabe KK, Souba WW (1996) Glutamine as a regulator of DNA and protein biosynthesis in human solid tumor cell lines. Ann Surg 224:189–197
12. Qu W, Zha Z, Ploessl K, Lieberman BP, Zhu L, Wise DR, B. Thompson C, Kung HF (2011) Synthesis of optically pure 4-fluoroglutamines as potential metabolic imaging agents for tumors. J Am Chem Soc 133:1122–1133
13. Lieberman BP, Ploessl K, Wang L, Qu W, Zha Z, Wise DR, Chodosh LA, Belka G, Thompson CB, Kung HF (2011) PET imaging of glutaminolysis in tumors by ^{18}F-(2S,4R)4-fluoroglutamine. J Nucl Med 52:1947–1955
14. Venneti S, Dunphy MP, Zhang H, Pitter KL, Zanzonico P, Campos C, Carlin SD, la Rocca G, Lyashchenko S, Ploessl K, Rohle D, Omuro AM, Cross JR, Brennan CW, Weber WA, Holland EC, Mellinghoff IK, Kung HF, Lewis JS, Thompson CB (2015) Glutamine-based PET imaging facilitates enhanced metabolic evaluation of gliomas in vivo. Sci Transl Med 7:274ra17
15. Zhou R, Pantel AR, Li S, Lieberman BP, Ploessl K, Choi H, Blankemeyer E, Lee H, Kung HF, Mach RH, Mankoff DA (2017) ^{18}F(2S,4R)-4-fluoroglutamine PET detects glutamine pool size changes in triple-negative breast cancer in response to glutaminase inhibition. Cancer Res 77:1476–1484
16. Zhu L, Ploessl K, Zhou R, Mankoff D, Kung HF (2017) Metabolic imaging of glutamine in cancer. J Nucl Med 58:533–537
17. Liu Y, Asai T, Nimer SD (2010) Myelodysplasia: battle in the bone marrow. Nat Med 16:30–32
18. Weinzierl EP, Arber DA (2013) The differential diagnosis and bone marrow evaluation of new-onset-pancytopnia. Am J Clin Pathol 139:9–29
19. Kawaguchi T, Nakakuma H (2007) New insights into molecular pathogenesis of bone marrow failure in paroxysmal nocturnal hemoglobinuria. Int J Hematol 86:27–32
20. Brown KE, Young NS (1996) Parvoviruses and bone marrow failure. Stem Cells 14:151–163
21. Abella E, Feliu E, Granada I, Millá F, Oriol A, Ribera JM, Sánchez-Planell L, Berga L, Reverter JC, Rozman C (2002) Bone marrow changes in anorexia nervosa are correlated with the amount of weight loss and not with other clinical findings. Am J Clin Pathol 118:582–588
22. Hassanein M, Hight MR, Buck JR, Tantawy MN, Nickels ML, Hoeksema MD, Harris BK, Boyd K, Massion PP, Manning HC (2016) Preclinical evaluation of 4-^{18}F-fluoroglutamine PET to assess ASCT2 expression in lung cancer. Mol Imaging Biol 18:18–23
23. Wu Z, Zha Z, Li G, Lieberman BP, Choi SR, Ploessl K, Kung HF (2014) ^{18}F-(2S,4S)-4-(3-fluoropropyl)glutamine as a tumor imaging agent. Mol Pharm 11:3852–3866
24. Martínez R, Chacón-García L (2005) The search of DNA-intercalators as antitumoral drugs: what it worked and what did not work. Curr Med Chem 12:127–151
25. Tewey KM, Rowe TC, Yang L et al (1984) Adriamycininduced DNA damage mediated by mammalian DNA topoisomerase II. Science 26:466–468
26. Lei H, Wang X, Wu C et al (2012) Early stage intercalation of doxorubicin to DNA fragments observed in molecular dynamics binding simulations. J Mol Graph Model 38:279–289
27. Pavanello F, Zucca E, Ghielmini M (2017) Rituximab: 13 open questions after 20years of clinical use. Cancer Treat Rev 53:38–46
28. Jager U, Fridrik M, Zeitlinger M, Heintel D, Hopfinger G, Burgstaller S, Mannhalter C, Oberaigner W, Porpaczy E, Skrabs C, Einberger C, Drach J, Raderer M, Gaiger A, Putman M, Greil R, for the Arbeitsgemeinschaft Medikamentose Tumortherapie (AGMT) Investigators (2012) Rituximab serum concentrations during immunochemotherapy of follicular lymphoma correlate with patient gender, bone marrow infiltration and clinical response. Haematologica 97:1431–1438
29. Pettengell R, Schmitz N, Gisselbrecht C, Smith G, Patton WN, Metzner B, Caballero D, Tilly H, Walewski JA, Bence-Bruckler I, To B, Geisler CH, Schots R, Kimby E, Taverna CJ, Kozák T, Dreger P, Uddin R, Ruiz de Elvira C, Goldstone AH (2013) Rituximab purging and/or maintenance in patients undergoing autologous transplantation for relapsed follicular lymphoma: a prospective randomized trial from the lymphoma working party of the European group for blood and marrow transplantation. J Clin Oncol 31:1624–1630
30. Piert M, Zittel TT, Machulla HJ, Becker GA, Jahn M, Maier G, Bares R, Becker HD (1998) Blood flow measurements with [(^{15})O]H2O and [^{18}F]fluoride ion PET in porcine vertebrae. J Bone Miner Res 13:1328–1336